Chinese Chemical Letters 35 (2024) 108380

Contents lists available at ScienceDirect

Chinese Chemical Letters

journal homepage: www.elsevier.com/locate/cclet

Studying the variable energy band structure for energy storage materials in charge/discharge process

Xuancheng Chen[a], Yu Huan[a,*], Ningqiang Sun[a], Yuanhui Su[a], Xuesong Shen[b], Guoqing Li[a], Jiaqi Zhang[a], Tao Wei[a,*]

[a] University of Jinan, Ji'nan 250022, China
[b] Weichai Power Co., Ltd., Weifang 261061, China

ARTICLE INFO

Article history:
Received 14 February 2023
Revised 10 March 2023
Accepted 24 March 2023
Available online 26 March 2023

Keywords:
Variable energy band structure
Energy storage materials
Charge-discharge process
Optical spectroscopy
Supercapacitors

ABSTRACT

So far, a clear understanding about the relationship of variable energy band structure with the corresponding charge-discharge process of energy storage materials is still lacking. Here, using optical spectroscopy (red-green-blue (RGB) value, reflectivity, transmittance, UV–vis, XPS, UPS) to study α-$Co(OH)_2$ electrode working in KOH electrolyte as the research object, we provide direct experimental evidence that: (1) The intercalation of OH^- ions will reduce the valence/conduction band (VB and CB) and band gap energy (E_g) values; (2) The deintercalation of OH^- ions corresponds with the reversion of VB, CB and E_g to the initial values; (3) The color of $Co(OH)_2$ electrode also exhibit regular variations in RGB value during the charge-discharge process.

Nowadays, with the rapid development of human society, the exploration of green, economic and sustainable energy storage devices has become an indispensable demand. At present, the most studied energy storage devices mainly include various batteries and capacitors, such as lithium-ion batteries, sodium-ion batteries, zinc-ion batteries, electric double-layer capacitors, and pseudocapacitors [1–9]. For energy storage devices, one of the most important components is their various energy storage materials. Such as for lithium-ion batteries, the energy storage materials include the widely studied $LiCoO_2$- or $LiFePO_4$-based cathode materials and the graphite or silicon-based anode materials [10–12]. For supercapacitors, the electrode materials mainly include carbon material, metal oxide, and conductive polymer [13–15]. To pursue energy storage materials with greater capacity, high power, better safety and non-pollution, it is also necessary to develop various testing techniques to systematically evaluate the energy storage materials/devices. For example, the cyclic voltammetry (CV) and galvanostatic charge-discharge (GCD) testing techniques can be used to characterize the charge-discharge voltage, capacity, rate, cycle and other properties of energy storage materials. The variations of morphology and volume of energy storage materials before, during and after charging and discharging process can be intuitively described by scanning electron microscope (SEM) and atomic force microscope (AFM). Park *et al.* clearly characterized the volume increase and shrinkage, and the damage of the silicon-based lithium-ion battery anode particles during the charging and discharging process by SEM technology [16]. The change of aliovalent cation valence state and the oxygen vacancy concentration in energy storage materials can be (semi-)quantitatively evaluated by XPS, EPR and chemical titration methods [17,18]. For different charge carriers charging/discharging in energy storage materials, the possible insertion site, transport route and activation energy can be calculated by theoretical computation. For example, the voltage profile for the discharge/charge curves can be described by the density-of-state diagram, which is mainly based on the corresponding positions of the bottom/top band gap and the aliovalent cation redox couples relative to the Fermi energy of lithium [19]. The possible changes in the crystal structure, bond length/angle, phase transition, *etc.* of energy storage materials during the charge and discharge process also can be characterized by XRD, TEM and Raman testing techniques [20–22]. Despite much progress, as mentioned above, has been made in the past decades to get a more accurate assessment for energy storage materials, however, a clear understanding of the relationship between the charge-discharge process of energy storage materials and the corresponding changes of energy band structure is still lacking.

In this work, an energy storage electrode cobalt hydroxide α-$Co(OH)_2$ with low cost, environmentally benign and high theoretical specific capacitance was chosen as research object. We studied

* Corresponding authors.
E-mail addresses: mse_huany@ujn.edu.cn (Y. Huan), mse_weit@ujn.edu.cn (T. Wei).

https://doi.org/10.1016/j.cclet.2023.108380
1001-8417/

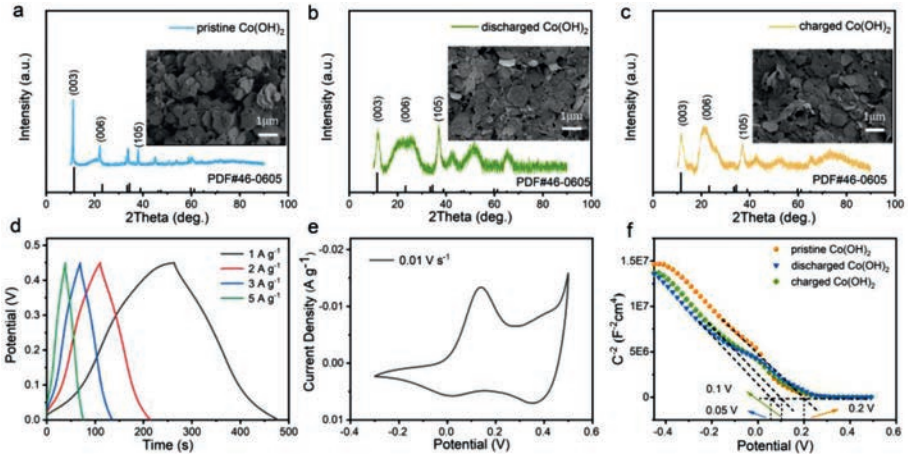

Fig. 1. XRD pattersns and SEM images of (a) $Co(OH)_2$, (b) discharged $Co(OH)_2$ and (c) charged $Co(OH)_2$ samples. (d) Galvanostatic charge/discharge curves of $Co(OH)_2$ (PVDF was added as a binder) at different current densities ranging from 1 A/g to 5 A/g. (e) CV curve of the $Co(OH)_2$ (PVDF was added as a binder) testing at 10 mV/s. (f) Mott–Schottky plots.

the charge-discharge process of energy storage materials by first revealing the regular variations of colors, optical spectrum and energy band structure. Their corresponding relationships provide a new perspective to study the insertion and removal of charge carriers in energy storage materials during the charge and discharge process.

The electrochemical properties of α-$Co(OH)_2$ electrode material are tested by forming a three-electrode configuration with Pt foil as the auxiliary electrode, Ag/AgCl as the reference electrode and 2 mol/L KOH solution as the electrolyte. Here, the initial $Co(OH)_2$ electrode is fabricated with 90 wt% pristine $Co(OH)_2$ powders + 10 wt% poly(vinylidene fluoride) (PVDF) coating on nickel foam. In charge-discharge process, the $Co(OH)_2$ electrode is discharged and charged to 0 V and 0.45 V respectively in a 2 mol/L KOH solution. In order to study the changes of $Co(OH)_2$ during discharging and discharging process, the pristine,discharged and charged $Co(OH)_2$ powders are collected and analyzed, respectively. As shown in Figs. 1a–c, the crystal structure and morphology of the three samples are characterized clearly. X-ray diffraction (XRD) evaluation results prove that all of the pristine, discharged and charged $Co(OH)_2$ samples appear in pure phase with characteristic peaks of $Co(OH)_2$. And the morphologies of the three $Co(OH)_2$ samples, as observed by field-emission scanning electron microscopy (FE-SEM), all show in hexagonal sheet structure, which is consistent with other reports [23]. No apparent XRD and SEM variations were observed from pristine to discharged and charged $Co(OH)_2$. All the GCD profiles are nonlinear and show obvious potential plateau (Fig. 1d), indicating that the charge storage of α-$Co(OH)_2$ electrode with (de)intercalating OH^- ions originated predominantly from Faradaic reaction [24]. The device exhibits a specific capacitance of 475 F/g at 1 A/g in accordance with Eq. 1 [25].

$$C_m = \frac{I \times \Delta t}{\Delta V \times m} \tag{1}$$

Furtherly, the shapes of GCD curves remain unchanged and keep symmetric with current densities increasing from 1 A/g to 5 A/g, which proves the good reversibility and rate capability of $Co(OH)_2$ electrode. The CV curve of α-$Co(OH)_2$ electrode with scan voltage from –0.3 V to +0.5 V and scan rate at 10 mV/s also shows obvious redox peaks (Fig. 1e), which corresponds to the potential of charge-discharge behavior in GCD curves. By comparing the cycled capacity for more than 2000 cycles, the excellent long-term stability means the good redox reversibility while $Co(OH)_2$ using as energy storage electrode (Fig. S2 in Supporting information). In addition, adding 10 wt% super P carbon black (SP) as conductor, the composite electrode demonstrates superior electrochemical performance (Figs. S3–S6 in Supporting information). As shown in Fig. 1f, the $Co(OH)_2$ coated on nickel foam is tested by electrochemical Mott–Schottky plots in 2 mol/L KOH solution. The result shows that the E_{fb} values of the pristine, discharged and charged samples are 0.2, 0.05 and 0.1 V, respectively. The measured flat-band voltage reflects the change of valence state of the three samples, which also proves that $Co(OH)_2$ undergoes the redox reactions during the charging and discharging process.

Furtherly, during the charging-discharging process, the color variation of $Co(OH)_2$ samples was recorded by Spectrophotometric colorimeter. As shown in Fig. 2a, its red-green-blue (RGB) value varies regularly with the corresponding GCD curves (presented by the black dots linked with broken black lines). For the pristine $Co(OH)_2$ powders, its RGB value is in (147, 186, 139). The initial $Co(OH)_2$ electrode (90 wt% $Co(OH)_2$ + 10 wt% PVDF coating on nickel foam) was infiltrated into 2 mol/L KOH solution elec-

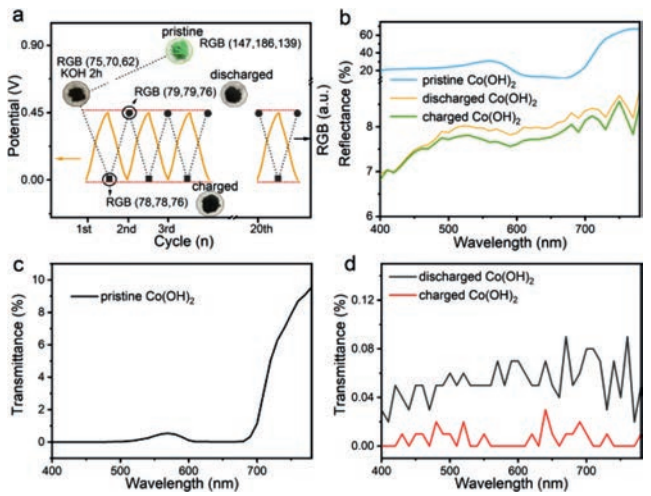

Fig. 2. Color change, reflection and transmissivity spectrum of cobalt hydroxide during the charging and discharging process. (a) Evaluation of $Co(OH)_2$ electrode by Galvanostatic charge/discharge curves testing at a current density of 1 A/g and the corresponding regular variations of color RGB value of discharged and charged $Co(OH)_2$ powders. The insertion is the optical images of pristine, discharged and charged $Co(OH)_2$ powders. (b) The reflectivity of pristine, discharged and charged $Co(OH)_2$ samples in relation to emitted wavelength. (c, d) The transmissivity of pristine $Co(OH)_2$, discharged $Co(OH)_2$ and charged $Co(OH)_2$ samples in relation to emitted wavelength.

trolyte for 2 h, and its RGB value is in (75, 70, 62). Furtherly, the discharged $Co(OH)_2$ electrode (with voltage at 0 V) with saturated KOH solution shows the color in RGB value (79, 79, 76). For $Co(OH)_2$ electrode charged to 0.45 V, OH^- as charge carriers were inserted into the interlayer structure of α-$Co(OH)_2$. The redox reaction is as follows (Eq. 2) [26].

$$Co(OH)_2 + OH^- \rightleftharpoons CoOOH + H_2O + e^- \quad (2)$$

With the introduction of OH^- ions, $Co(OH)_2$ was oxidized to CoOOH, which leads the color of charged $Co(OH)_2$ electrode varying to the RGB value (78, 78, 76). For $Co(OH)_2$ electrode discharging to 0 V, the OH^- ions were taken off from the interlayer. The corresponding RGB value of the discharged $Co(OH)_2$ electrode was recovered to (79, 79, 76) again. And the corresponding RGB values of $Co(OH)_2$ electrode also were recorded for 20 cycles. As shown in Fig. 2a, the changes of the obtained color vary regularly during the charge-discharge process, which is consistent with the excellent capacitance stability.

In addition, the optical images for pristine $Co(OH)_2$ powders, discharged and charged $Co(OH)_2$ electrode powders (Fig. S1 in Supporting information) are inserted into Fig. 2a to compare the color variation. The color of pristine $Co(OH)_2$ powders is green, corresponding with its RGB value. In the macroscopic view, the color of discharged/charged $Co(OH)_2$ electrode powders is obviously different from pristine powder, both showing in black gray, which is consistent with their RGB values. For $Co(OH)_2$ + PVDF + SP electrode, its RGB values and optical images also vary regularly with the GCD curves (Fig. S7 in Supporting information).

The varied colors of $Co(OH)_2$ samples under the charge-discharge process can be reflected by detecting their varied optical properties, such as reflection, refraction and transmission [27]. For pristine $Co(OH)_2$, the powder is pressed into circular flakes with a certain diameter and thickness to test its reflectance, and the reflectance is obtained by the Spectrophotometer colorimeter. As shown in Fig. 2b, the reflectance of pristine green $Co(OH)_2$ powder varies from 20% to 70% with the test wavelength switching from 400 nm to 780 nm. For $Co(OH)_2$ electrodes, with the electrode sheet ($Co(OH)_2$ powder coated on nickel foam) discharging/charging to 0/0.45 V, the corresponding reflectance can be recorded. The $Co(OH)_2$ electrode in black gray absorbed most of the exciting light, herein, its reflectivity is significantly lower than pristine $Co(OH)_2$, less than 10%. Moreover, for semiconductors, the wider band gap corresponds with less absorbance for white exciting light [28,29]. Herein, the higher reflection coefficient for discharged $Co(OH)_2$ electrode (than charged electrode) means bigger band gap.

For polycrystalline semiconductor materials, their optical properties are mainly affected by scattering and reflection, and are almost opaque to exciting light. However, evaluating the variation of transmittance is still an effective way to reveal the changed band gap from pristine to discharged and charged $Co(OH)_2$. To measure the light transmittance, 90 wt% $Co(OH)_2$ and 10 wt% PVDF are coated on FTO conductive glass to form a thin and uniform film as working electrode, which ensures the transmission of light. The electrode is charged and discharged to 0.45 and 0 V, and then the transmittance is measured after drying. As shown in Figs. 2c and d, the transmittance of pristine $Co(OH)_2$ varies between 1 and 10%, while discharged $Co(OH)_2$ and charged $Co(OH)_2$ transmissivity is less than 0.1%. The significantly higher transmittance for pristine $Co(OH)_2$ means larger band gap (for exciting light passing through) than discharged and charged $Co(OH)_2$. Furtherly, the comparison of transmittance in Fig. 2d represents that discharged $Co(OH)_2$ has the larger band gap than charged $Co(OH)_2$, which can be explained by the higher transmittance.

For semiconductors, the color variation corresponds to the variation of band gap energy (E_g) value. Herein, the changed color (or RGB value) of $Co(OH)_2$ samples can be evaluated by the ultraviolet-visible spectroscopy, which can give the variation of E_g value. Fig. 3 is the UV–vis spectra of $Co(OH)_2$ samples with the absorption wavelength ranging from 300 nm to 800 nm. For pristine $Co(OH)_2$ powders (Fig. 3a), the strong absorption wavelength ranges from 560 nm to 680 nm, and the absorption peak at around 550 nm results in the dominant green color [30]. Then, the E_g value can be calculated by Tauc's plot and expressed using the following Eq. 3 [31].

$$(ah\nu)^n = k(h\nu - E_g) \quad (3)$$

The calculated E_g value for pristine $Co(OH)_2$ is 2.85 eV, shown in the insert chart of Fig. 3a. For PVDF binder, the calculated E_g value is 3.54 eV (Fig. 3b). For $Co(OH)_2$ + PVDF electrode, the calculated UV–vis spectra shows two individual E_g values at 3.54 and 2.85 eV, which means the E_g values of $Co(OH)_2$ samples are unaffected by the introduction of PVDF binder (Figs. 3c and d). For $Co(OH)_2$ + PVDF + SP electrode, the absorption peaks of $Co(OH)_2$ and PVDF are covered by the introduced SP carbon black (Fig. S8 in Supporting information). Herein, the optical spectroscopy was conducted with $Co(OH)_2$ + PVDF as the working electrode.

To obtain the E_g value of discharged and charged $Co(OH)_2$ powders, the initial $Co(OH)_2$ sample was coated on FTO conductive glass as a working electrode and then the electrode was charged/discharged in 2 mol/L KOH solution electrolyte. After the electrode was charged and discharged to 0.45 and 0 V individually, the corresponding $Co(OH)_2$ electrode sheet is rinsed gently with deionized water, subsequently dried in an oven at 75 °C. The dried charged/discharged $Co(OH)_2$ powders are scraped from conductive glass to test the E_g value. Figs. 3e and f show the absorption peaks and the corresponding Tauc plot of discharged and charged $Co(OH)_2$ powders. It is observed that the range of strong absorption peaks of the two samples is much different with pristine $Co(OH)_2$ powders. We think the main reason is the adsorption (or chemical reaction) of OH^- ions with $Co(OH)_2$ particles. The strong absorption peaks of the two samples both appear around 680 nm, corresponding with the gray-black color. Furtherly, the calculated E_g for discharged $Co(OH)_2$ electrode powders is 1.94 eV. For charged $Co(OH)_2$ electrode powders, the calculated E_g was reduced furtherly to 1.75 eV. This means the intercalation/deintercalation of OH^- ions during the charge and discharge process causes further change of E_g of $Co(OH)_2$ electrode. From discharged to charged $Co(OH)_2$, the smaller E_g was explained: for p-type $Co(OH)_2$ semiconductor, we think the intercalation of OH^- ions will produce impurity level near the VB, which causes the further reduction of E_g.

In order to construct the schematic diagram of energy band structure, the valence band potential ($E_{VB,XPS}$) of pristine, discharged and charged $Co(OH)_2$ samples were measured *via* X-ray photoelectron spectroscopy (XPS) analysis. And the XPS absorption spectra of the three samples as a function of binding energy were shown in Figs. 4a–c. The VB positions of the $Co(OH)_2$ samples are calculated by linear extrapolation of the valence band leading edge with the corresponding baseline of the background signal [32].

According to the test results, the corresponding $E_{VB,XPS}$ of pristine, discharged and charged $Co(OH)_2$ samples is measured to be 0.97, 0.09 and 0.23 eV. Then, the E_{VB} values of the corresponding standard hydrogen electrode ($E_{VB,NHE}$) can be obtained by to the following Eq. 4.

$$E_{VB,NHE} = \varphi + E_{VB,XPS} - 4.44 \quad (4)$$

φ is the work function of the instrument (4.72 eV) [33]. As a result, the $E_{VB,NHE}$ of the three samples is calculated to be 1.25, 0.37 and 0.51 eV, respectively. For the sake of unity with band gap, the $E_{VB,NHE}$ is converted into solid physical energy level scales (vacuum level) for comparison. Finally, the valence band value of the pristine, discharged and charged $Co(OH)_2$ is calculated to be –5.69,

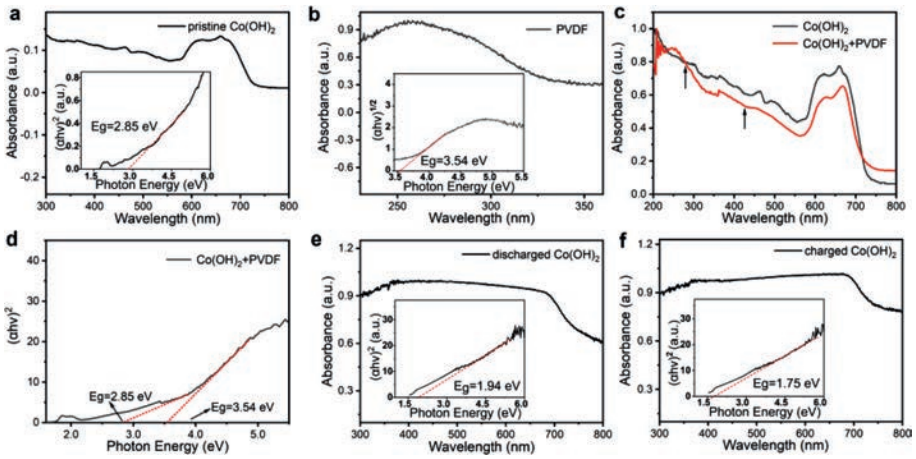

Fig. 3. (a, b) UV–vis diffuse reflectance spectra of pristine and PVDF powders and the corresponding plot of transformed Kubelka-Munk function *versus* the varied energy of emitting light. (c) UV–vis diffuse reflectance spectra of $Co(OH)_2$ and $Co(OH)_2$ + PVDF powders. (d) Tauc plots of $Co(OH)_2$ + PVDF powders. (e, f) UV–vis diffuse reflectance spectra of discharged and charged $Co(OH)_2$ powders and the corresponding plot of transformed Kubelka-Munk function versus the varied energy of emitting light.

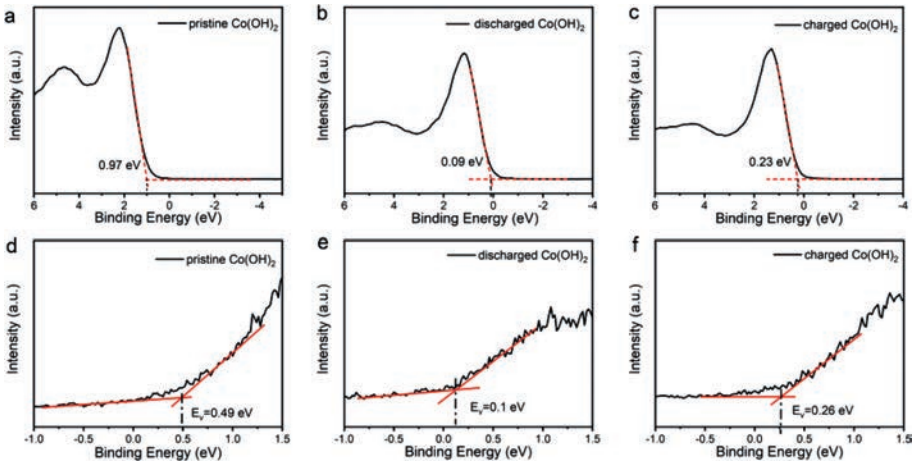

Fig. 4. (a–c) Valence band potential of pristine, discharged and charged $Co(OH)_2$ samples evaluated by X-ray photoelectron spectroscopy. (d–f) Low-band energy slope of the ultraviolet photon electron spectroscopy spectra of pristine, discharged and charged $Co(OH)_2$ samples.

−4.81 and −4.95 eV, respectively, according to the conversion Eq. 5 [34].

$$E_{vac} = -4.44 - eE_{NHE} \quad (5)$$

First, the valence band value of discharged/charged $Co(OH)_2$ electrodes is more positive than pristine $Co(OH)_2$, which was also attributed to the adsorption (or chemical reaction) of OH^- ions with $Co(OH)_2$ particles. Second, the intercalation/deintercalation of OH^- ions in $Co(OH)_2$ electrode will introduce new filled/empty electronic states at or around the VB maximum, which sheds light on the change of valence band values. Here, from the discharged to charged electrode, the intercalation of OH^- ions will oxidize $Co^{2+}(OH)_2$ to $Co^{3+}OOH$. So the further spillover of electrons from Co^{3+} ions of $Co^{3+}OOH$ needs higher energy (work function, W_F), which explains the more negative E_{vac} of charged $Co(OH)_2$ than discharged $Co(OH)_2$ (Figs. 4b and c).

To further verify the accuracy of changed $E_{VB,XPS}$ as evaluated by XPS technology, we also use the ultraviolet photon electron spectroscopy (UPS) and electrochemical Mott–Schottky equation to further determine the band edges of $Co(OH)_2$ electrode under charging and discharging process. UPS is a widely used way which probes the electronic VB [35]. It measures the kinetic energy of photoelectrons emitted by solid surfaces under the irradiation of ultraviolet light, which provides the distribution of electron density in the VB as well as on the W_F. The UPS test was prepared by coating $Co(OH)_2$ on FTO conductive glass to form a thin and uniform film electrode [36]. The charge-discharge process of the thin film electrode is carried out in a 2 mol/L KOH solution by a three-electrode test device. Figs. 4d–f show the low binding energy slopes of pristine, discharged and charged $Co(OH)_2$ samples. The intersection of the slope curve is the VB maximum below Femi level. It is calculated that the VB of the three samples is 0.49, 0.1 and 0.26 eV, respectively. The W_F is defined as the energy difference from the Fermi level to the vacuum energy level. In the UPS spectrum, it can be calculated from the difference between the energy of the UV photons and the secondary electron cutoff (high-binding energy (BE) cutoff) [37]. The cut-off energy of the three samples is 16.01, 15.96 and 15.98 eV (Fig. S9 in Supporting information). Furthermore, the W_F can be calculated by the following Eq. 6.

$$W_F = h\nu - (BE_{max} - E_F) \quad (6)$$

$h\nu$ is the energy of the *He I* ultraviolet photon source (21.22 eV), $BE_{max} = E_{cutoff}$. It can be assumed that $E_F = 0$ by calibrating the energy spectrum scale of the spectrum. Therefore, the W_F of the three materials can be calculated as 5.21, 5.26 and 5.24 eV. Herein, the energy band structure relative to the energy level of the solid physical scale can be obtained according to the W_F and $E_{VB,UPS}$. The valence band positions relative to the vacuum level can be obtained as −5.70, −5.36 and −5.50 eV, respectively.

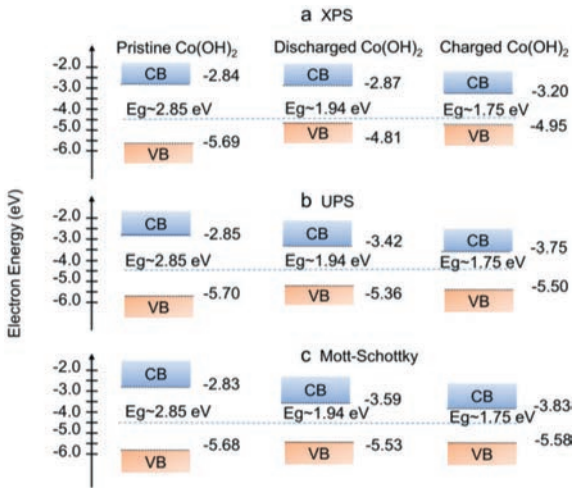

Fig. 5. Band structure diagram. Position of E_{CB} (blue) and E_{VB} (orange) for pristine, discharged and charged $Co(OH)_2$ samples calculated from the optical band gap and the (a) VB-XPS, (b) UPS and (c) Mott–Schottky plots.

For semiconductor-like materials, the Mott–Schottky equation can be used to measure the flat band potential (E_{fb}) at the electrode-electrolyte interface, which then was used to reflect the valence/conduction band values. Herein, the testing system for E_{fb} was prepared with $Co(OH)_2$ coating on nickel foam as working electrode with Ag/AgCl as reference electrode and with 2 mol/L KOH solution as electrolyte. In the Mott–Schottky test, the voltage range is –0.45 V to 0.5 V and the frequency is 1000 Hz. As shown in Fig. 1f, the E_{fb} is determined by the x-intercept (potential axis) of the tangent line of the Mott–Schottky plot. The result shows that the E_{fb} values of the pristine, discharged and charged samples are 0.2, 0.05 and 0.1 V, respectively. It is evident that the slope of the tangent line is negative, suggesting α-$Co(OH)_2$ a p-type semiconductor [38–40]. There is a certain relationship between the valence band value and the varied flat band voltage (Eq. 7).

$$E_V = E_{fb} + kT\ln(N_A/N_V) \quad (7)$$

E_{fb} is the flat band potential, N_A is the volume carrier density, N_V is the valence band effective state density, k is the Boltzmann constant and T is the temperature in absolute scale. The second term depends on the doping concentration, which for semiconductors is usually 0.1–0.2 eV and is negligible. Herein, we ignore the second term to compare the change of valence band values.

Then, we convert the valence bands into the solid physical level scale (vacuum level) according to Eqs. 5 and 8 [34,41].

$$E_{NHE} = E_{Ag/AgCl} + 0.059pH + 0.199 \quad (8)$$

pH value is 14.3 for 2 mol/L KOH electrolyte. The calculated final valence band value of the three samples is –5.68, –5.53 and –5.58 eV, respectively. Herein, in the process of the Mott–Schottky test, $Co(OH)_2$ may react with KOH solution with the increase of testing voltage, which would affect the flat band potential (valance band) in a certain state. For example, although the trend of the obtained valence band position by the Mott–Schottky equation is still upward from pristine to charged/discharged $Co(OH)_2$ samples, the concrete data does not change much as compared with XPS and UPS results.

Fig. 5 draws a comparison of the band diagrams for pristine, discharged and charged $Co(OH)_2$ samples based on the results of UV–vis spectrum, XPS, UPS and Mott–Schottky plot. And the calculating formula is as follows (Eq. 9) [28].

$$E_{CB} = E_{VB} - E_g \quad (9)$$

Fig. 5a is a schematic diagram of the energy bands obtained by XPS and UV–vis tests. The calculated VB, CB and E_g of pristine $Co(OH)_2$ are –5.69, –2.84 and 2.85 eV, which are in line with the existing research results [42,43]. For discharged $Co(OH)_2$ electrode, with the adsorption (or chemical reaction) of OH^- ions with $Co(OH)_2$ particles, the calculated VB increased to –4.81 eV. At the same time, the CB and E_g values were reduced to –2.87 and 1.94 eV.

For charged $Co(OH)_2$ electrode, the present study has demonstrated that the charging process of α-$Co(OH)_2$ is processed by OH^- intercalation [44]. The intercalation of OH^- ions further reduces the VB, CB and E_g values of charged $Co(OH)_2$ electrode to –4.95, –3.20 and 1.75 eV (compared with –4.81, –2.87 and 1.94 eV of discharged $Co(OH)_2$). Figs. 5b and c are the schematic band diagrams of VB, CB and E_g values obtained by UPS/UV–vis and Mott–Schottky/UV–vis tests. The calculated results for pristine, discharged and charged $Co(OH)_2$ samples are basically same with the XPS/UV–vis results. As discussed above, the apparent variation of $Co(OH)_2$ energy band structure from pristine powders to charged/discharged electrodes was attributed to the adsorption (or chemical reaction) of OH^- ions with $Co(OH)_2$ particles. The varied energy band structure from discharged to charged $Co(OH)_2$ can be explained by the reversible Faradaic reaction. As shown in Table S1 (Supporting information), the XPS results reveal the coexistence of Co^{2+} and Co^{3+} ions in discharged and charged $Co(OH)_2$. The calculated Co^{2+}/Co^{3+} ratios are 2.07 and 0.53 in discharged and charged samples. During the charging and discharging process, the intercalation/deintercalation of OH^- ions from the interlayers of $Co(OH)_2$ electrode will oxidize/reduce more $Co^{2/3+}$ to $Co^{3/2+}$, which causes changes in the energy band structure. Recently, Gabrelian *et al.* have studied the valence-band electronic structure and main optical properties of $Cu_2HgGeTe_4$ materials by theoretical simulation within a DFT framework and experimental XPS [45], and the obtained trend is consistent with the varied VB and CB of Co ion as studied in this work.

In this work, by combining optical spectroscopy characterization with electrochemical studies, we have demonstrated that the charge-carrier intercalation/deintercalation in energy storage materials not only governs the variations of color RGB values but also the energy band structure. Specifically, with $Co(OH)_2$ electrode working in KOH electrolyte as an example, the VB, CB and E_g values show apparent reduction/increment with OH^- ions intercalating or taking off from its interlayer structure. In addition, the intercalation/deintercalation of OH^- ions also triggered the redox reaction of Co^{2+} and Co^{3+} ions, resulting in the regular variation of RGB values. This work provides a feasible way to characterize the changes of energy band structure during the charge-discharge process by optical spectroscopy, which is helpful for the design of high-performance energy storage materials.

Declaration of competing interest

The authors declare that they have no known competing financial interests or personal relationships that could have appeared to influence the work reported in this paper.

Acknowledgment

This work was supported by the National Natural Science Foundation of China (Nos. 51972146, 52072150).

Supplementary materials

Supplementary material associated with this article can be found, in the online version, at doi:10.1016/j.cclet.2023.108380.

References

[1] A. Manthiram, ACS Cent. Sci. 3 (2017) 1063–1069.
[2] G.Q. Li, M.Y. Ma, X.C. Chen, et al., Energy Fuels 37 (2023) 702–710.
[3] J.Y. Hwang, S.T. Myung, Y.K. Sun, Chem. Soc. Rev. 46 (2017) 3529–3614.
[4] L.Q. Mai, A. Minhas-Khan, X. Tian, K.M. Hercule, et al., Nat. Commun. 4 (2013) 2923.
[5] C.G. Wang, P.X. Sun, G.M. Qu, et al., Chin. Chem. Lett. 29 (2018) 1731–1740.
[6] M.R. Guo, J. Zhan, Z.K. Wang, et al., Chin. Chem. Lett. 34 (2023) 107709.
[7] N.N. Yang, L. Ji, H.C. Fu, et al., Chin. Chem. Lett. 34 (2022) 3961–3967.
[8] X.W. Wang, Y.C. Sun, W.C. Zhang, et al., Chin. Chem. Lett. 34 (2023) 107593.
[9] Q. Xia, T. Xia, X. Wu, et al., Rare Met. 41 (2022) 1195–1201.
[10] N. Balke, S. Jesse, A.N. Morozovska, et al., Nat. Nanotechnol. 5 (2010) 749–754.
[11] W. Kim, W. Ryu, D. Han, et al., ACS Appl. Mater. Interfaces 6 (2014) 4731–4736.
[12] Y. Son, N. Kim, T. Lee, et al., Adv. Mater. 32 (2020) e2003286.
[13] S.M.Y. Zhu, M.D. Stoller, K.J. Ganesh, et al., Science 24 (2011) 1537–1541.
[14] H. Gao, F. Xiao, C.B. Ching, et al., ACS Appl. Mater. Interfaces 4 (2012) 2801–2810.
[15] D. Sheberla, J.C. Bachman, J.S. Elias, et al., Nat. Mater. 16 (2017) 220–224.
[16] H. Park, S. Choi, S. Lee, et al., J. Mater. Chem. A 3 (2015) 1325–1332.
[17] G. Li, K. He, F. Zhang, et al., Appl. Catal. B: Environ. 309 (2022) 121231.
[18] W.C. Huo, X.A. Dong, J.Y. Li, et al., Chem. Eng. J. 361 (2019) 129–138.
[19] J.B. Goodenough, Y. Kim, Chem. Mater. 22 (2009) 587–603.
[20] W. Yao, A.R. Armstrong, X. Zhou, et al., Nat. Commun. 10 (2019) 3483.
[21] L. Feng, Y. Liu, L. Wu, et al., J. Alloy. Compd. 881 (2021) 160626.
[22] Q.F. Xiao, M. Gu, H. Yang, et al., Nat. Commun. 6 (2015) 8844.
[23] K. Ding, X. Zhang, J. Li, et al., CrystEngComm 19 (2017) 5780–5786.
[24] U.M. Patil, M.S. Nam, J.S. Sohn, et al., J. Mater. Chem. A 2 (2014) 19075–19083.
[25] X. Wu, L. Meng, Q. Wang, et al., Sol. Energy Mater. Sol. Cells 174 (2018) 325–332.
[26] A.D. Jagadale, V.S. Kumbhar, D.S. Dhawale, et al., Electrochim. Acta 98 (2013) 32–38.
[27] M.G. Berhe, H.G. Oh, S.K. Park, et al., J. Mater. Res. Technol. 16 (2022) 322–334.
[28] F.P. Hagen, D. Kretzler, T. Häber, et al., Carbon 182 (2021) 634–654.
[29] J.F. Luo, C.Q. Xie, S.L. Pan, et al., J. Quant. Spectrosc. Radiat. Transf. 287 (2022) 108228.
[30] Z.L.R. Ma, K. Takada, K. Fukuda, et al., Inorg. Chem. 61 (2006) 3964–3969.
[31] I. Thaheem, K.J. Kim, J.J. Lee, et al., J. Mater. Chem. A 7 (2019) 19696–19703.
[32] H. Li, X. Liu, L. Sang, et al., Phys. Status Solidi 251 (2014) 788–791.
[33] X. Li, B. Kang, F. Dong, et al., Nano Energy 81 (2021) 105671.
[34] S. Trasatti, Pure Appl. Chem. 58 (1986) 955–966.
[35] G. Xiong, R. Shao, T.C. Droubay, et al., Adv. Funct. Mater. 17 (2007) 2133–2138.
[36] C. Maheu, L. Cardenas, E. Puzenat, et al., Phys. Chem. Chem. Phys. 20 (2018) 25629–25637.
[37] P. Ramaswamy, S. Devkota, R. Pokharel, et al., Sci. Rep. 11 (2021) 8329–8342.
[38] M. Forghani, J. McCarthy, A.P. Cameron, et al., J. Electrochem. Soc. 168 (2021) 020508.
[39] M.A. Hughes, J.A. Allen, S.W. Donne, Electrochim. Acta 338 (2020) 135847.
[40] D.P. Sahoo, S. Nayak, K.H. Reddy, et al., Inorg. Chem. 57 (2018) 3840–3854.
[41] Z. Dong, D. Ding, T. Li, et al., Appl. Surf. Sci. 443 (2018) 321–328.
[42] M. Suksomboon, K. Kongsawatvoragul, S. Duangdangchote, et al., ACS Omega 6 (2021) 20804–20811.
[43] S. Kalasina, P. Pattanasattayavong, M. Suksomboon, et al., Chem. Commun. 53 (2017) 709–712.
[44] X. Li, L. Lu, J. Shen, et al., J. Power Sources 477 (2020) 228974.
[45] B.V. Gabrelian, A.A. Lavrentyev, Tuan.V. Vu, et al., Mater. Today Commun. 23 (2020) 100828.